Check for updates

Modeling and advanced exergy analysis of integrated reverse osmosis desalination with geothermal energy

R. Yargholi, H. Kariman, S. Hoseinzadeh, M. Bidi and A. Naseri

ABSTRACT

In this research, the integrated carbon dioxide power cycle with a geothermal energy source to supply the required reverse osmosis desalination power for freshwater production is defined. It is also a carbon dioxide power cycle, coupled with thermal energy recovery of infrared energy of liquid natural gas (LNG) to generate more power. A sodium hypochlorite generator is considered to prevent the brine water discharging. The brine water portion of the desalination outlet was the input to this generator. The cycling power is consumed by the desalination system and sodium hypochlorite generator. After modeling, the advanced exergy analyses are studied. By exergy analysis, it is observed that in this model the condenser has the highest exergy destruction rate, equal to 952 kW. Additionally, the unavoidable part of the exergy destruction of carbon dioxide turbine constitutes 88% of its exergy destruction that is equal to 301 kW. So this component is the best option to improve exergy destruction.

Key words | advanced exergy, CO_2 power cycle, reverse osmosis desalination, sodium hypochlorite generator

R. Yargholi
H. Kariman
M. Bidi
Faculty of Mechanical and Energy Engineering,
Shahid Beheshti University, A.C.,
Tehran,
Iran

S. Hoseinzadeh (corresponding author)
Centre for Asset Integrity Management,
Department of Mechanical and Aeronautical Engineering,
University of Pretoria,
Pretoria,
South Africa
E-mail: *hoseinzadeh.siamak@gmail.com*

A. Naseri
Department of Mechanical Engineering,
Faculty of Engineering,
The University of Auckland,
Auckland,
New Zealand

NOMENCLATURE

Q	heat transfer (kJ)
W	mechanical power output (kJ)
H	enthalpy (kJ/kg)
M^0	mass flow (kg/s)
R	global constants of gases (Lit.atm/mol.K^0)
T	flow temperatures (C°)
K_w	water permeability coefficient
P	pressure (MPa)
A_m	area of membrane (m)
X	concentration (g/L)
Ex	exergy (kJ)
MW	molar mass (mol)
r_k	exergy destruction (kJ)

GREEK LETTERS

η	efficiency (%)
π	osmotic pressure (atmosphere)
ρ	density (kg/m^3)

doi: 10.2166/ws.2020.021

INTRODUCTION

All human beings are now facing the challenge of the water crisis, or will face it in the near future. On the other hand, when we discuss the water crisis or water scarcity, it is actually a matter of fresh water. Certainly, human needs for water, the need of agriculture, and most of industry's need for water are needs for fresh water. There is still no crisis and shortage in the brine water sector. Thus, in geographical locations where brine water is available, part of the freshwater needs can be met using desalination systems. On the other hand, desalination plants, of course, need energy to perform their job and, as mentioned earlier, the use of geothermal energy can be a good option to supply this

Downloaded from http://iwaponline.com/ws/article-pdf/20/3/984/765699/ws020030984.pdf
by guest

energy. Desalination systems also have two freshwater and brine water outlets with concentrations higher than the inlet concentration. Now another issue that can be challenging is the brine water output of the system. Brine water discharge from the outlet of the desalination system to the seas in areas where discharge occurs increases salinity, creates water flow, and also increases seawater temperature and its opacity. These factors can damage the marine environment and cause fish to migrate and change the ecosystem of the area. Occasionally, micro elements and toxins appear in the salt solution (Al-Mutaz 1991). Therefore, the brine water from the desalination outlet can be used as the input for a sodium hypochlorite generator. This has the two advantages of not discharging brine water into the sea and producing sodium hypochlorite (with the trademark of Whitex) used as disinfectant. Sodium hypochlorite produced for disinfection and washing of desalination system components and other components of the same complex can be used.

Also, various analyses including exergy analysis, advanced exergy analysis and exergoeconomic analysis are performed for a deeper understanding and more detailed examination of this thermodynamic complex. Advanced exergy analysis can reveal how much exergy destruction in the system and its components can be improved. Exergoeconomic analysis can also provide useful information on the cost of system flows. This analysis is essential for optimal system design. Optimization of the proposed system is also done for more profitable utilization from economic and thermodynamic aspects.

Numerous studies have been conducted in the areas used in this title. Ali Nasseri presented a system for the simultaneous conversion of brine water to drinking water and hydrogen production using solar energy and the critical carbon dioxide cycle along with thermal recovery of infrared energy from natural liquid gas, and performed thermodynamic and exergy analysis of this system to investigate the effect of several thermodynamic parameters on the overall performance of the system. The results of his studies showed that the highest exergy destruction is associated with collectors and condensers, respectively. Also among the outlet flows, the natural gas emitted from the natural gas turbine has the highest output exergy. In addition, the carbon dioxide turbine inlet pressure has an optimal value to maximize the production and useful output power (Naseri *et al.* 2017a). He also investigated the exergy analysis of this system using a Stirling engine instead of a condenser. His results showed that replacing the condenser with a Stirling engine reduces the exergy destruction associated with the heat transfer from carbon dioxide to liquid natural gas (LNG) from 16.7% to 8.8% (Naseri *et al.* 2017b). Ehsan Akrami has designed a cycle including organic Rankine cycle, home water heater, absorption refrigeration cycle, and proton exchange membrane electrolyzer, for simultaneous generation of electricity, heating, cooling and hydrogen, and performed the energy analysis, exergy analysis and exergoeconomic analysis. He has also investigated the effects of some important variables such as geothermal water temperature and turbine inlet temperature and pressure on various parameters such as system energy and exergy efficiency, system output heating and cooling rate and hydrogen production. The results of his research showed that the energy and exergy efficiency of the proposed system are 34.98% and 49.17%, respectively and, assuming the fact that geothermal water temperature increases from 185 °C to 215 °C, the highest and lowest total unit costs are estimated to be $23.18 and $22.73, respectively (Akrami *et al.* 2017). Wang *et al.* investigated the parametric study of exergy of carbon dioxide power cycle utilizing dissipated heat as a heat source and optimized the thermodynamic parameters of the system by considering exergy efficiency as the objective function. The results of their studies showed that the optimum point in the cycle parameters with high accuracy can be obtained by neural network optimization. They also found that parameters such as the pressure and the inlet temperature of the turbine could have the greatest impact on the performance of the cycle (Wang *et al.* 2010). Kariman *et al.* explored a new type of industrial desalination equipment. It uses electrical energy to evaporate effluents and is environmentally friendly because of reclaimed wastewater. In this study, energy analysis was performed for the first time to identify important energy consuming equipment. Exergy analysis of the system showed that the most exergy destruction occurred in the boiler chamber and the central heat exchanger (Kariman *et al.* 2019a). They also studied different types of desalination systems and their governing equations, then modeled the energy consumption of the evaporation

Downloaded from http://iwaponline.com/ws/article-pdf/20/3/984/765699/ws020030984.pdf
by guest

vacuum evaporation system with a brine tank and reported on the economic analysis results (Hoseinzadeh & Azadi 2017; Yousef Nezhad & Hoseinzadeh 2017; Hoseinzadeh 2019; Hoseinzadeh *et al.* 2019a, 2019b, 2019c, 2019d; Javadi *et al.* 2019; Kariman *et al.* 2019b).

Wang performed the thermodynamic analysis and optimization of the supercritical carbon dioxide system fed by geothermal energy. His results showed that an increase in exergy efficiency would increase the rate of heat exchange per unit of power output (Wang *et al.* 2014). Mehdi Mehrpouya presented a new model including a solar collector system as a heat source for the system and a cycle of supercritical carbon dioxide power generation along with the use of LNG for cooling and studied its thermodynamics. The results of his investigations showed that the system performance could be improved by adjusting the inlet conditions of the turbine and the LNG coolant flow rate (Mehrpooya *et al.* 2016). Sun *et al.* presented hydrogen production by the power generated by the supercritical cycle of carbon dioxide fed by solar collectors and optimized the system using the PSO method. They showed that there is an optimum point for the inlet pressure of the turbine that can provide the highest exergy efficiency. They also calculated the hydrogen production rate by optimization by considering the appropriate operating conditions (Sun *et al.* 2012). Xia *et al.* optimized and thermodynamically investigated the supercritical cycle of carbon dioxide fed by the solar collector system for the production of water by reverse osmosis desalination system with infrared heat recovery of LNG and examined the effect of various thermodynamic parameters on the performance of the complex (Xia *et al.* 2014). Mahmoudi *et al.* performed thermodynamic analysis and multiobjective optimization of the hybrid complex including a molten carbonate fuel cell, supercritical carbon dioxide cycle and organic Rankine cycle. The results also showed that the most and the second greatest exergy destruction in such a complex occurs in the catalyst burner of the complex and the fuel cell (Mahmoudi & Ghavimi 2016). Mohammed Hossein Ahmadi *et al.* investigated the thermodynamics, exergy and exergoeconomics and optimization of the carbon dioxide cycle fed by the geothermal energy source and examined the results of the optimization with other related models and showed that the results obtained by the method used are acceptable. By applying the supercritical cycle of carbon dioxide as a PEM fuel cell cooling system (Ahmadi *et al.* 2016a, 2016b), they also demonstrated that, in the presented model, the output power is increased by 39% compared to fuel cells alone (Ahmadi *et al.* 2016c). Safaei *et al.* investigated the economics of exergy optimization, using the thermodynamic method to select the best thermodynamically and economically useful cycle. (Safaei *et al.* 2016; Arani *et al.* 2017; Behnampour *et al.* 2017; Keshavarzzadeh *et al.* 2019). For this purpose, some applied cycles were examined and then the lubrication cycle was selected (Abbassi *et al.* 2018; Abdollahi *et al.* 2018; Maleki *et al.* 2019). in addition, it was shown that very low and very high pressure rates were far from favorable conditions (Dadsetani *et al.* 2019; Sarafraz *et al.* 2019a, 2019b).

MODELING OF THE DESIRED CYCLE

Figure 1 provides a view of the model investigated in this study.

The model consists of geothermal energy sources, complexes of power generation, drinking water production, and sodium hypochlorite production. In the carbon dioxide generation cycle, the operating fluid in the steam generator receives its required heat from the geothermal energy source. So it reaches its supercritical state and, after generating power in the carbon dioxide turbine of this cycle, is condensed inside the condenser to enter the pump in the saturated liquid state. In order to absorb more heat from the steam generator, carbon dioxide enters the preheater before reaching the steam generator and after passing the pump, to enter the steam generator at a higher temperature. In the preheater, water enters the heat exchanger at an inlet temperature equal to the ambient temperature. Since the carbon dioxide is at a temperature below zero, the water gives its heat to the carbon dioxide and cools itself. Thus, the operating fluid of this cycle enters the steam generator at a higher temperature. Now because carbon dioxide is condensed at a temperature lower than the ambient temperature, it needs a cold source or another fluid at a lower temperature. Low-temperature LNG can be used as this cold source. Therefore, the operating fluid of LNG is pumped to the condenser in the carbon dioxide cycle in the LNG gasification complex, to absorb heat and condense

Downloaded from http://iwaponline.com/ws/article-pdf/20/3/984/765699/ws020030984.pdf
by guest

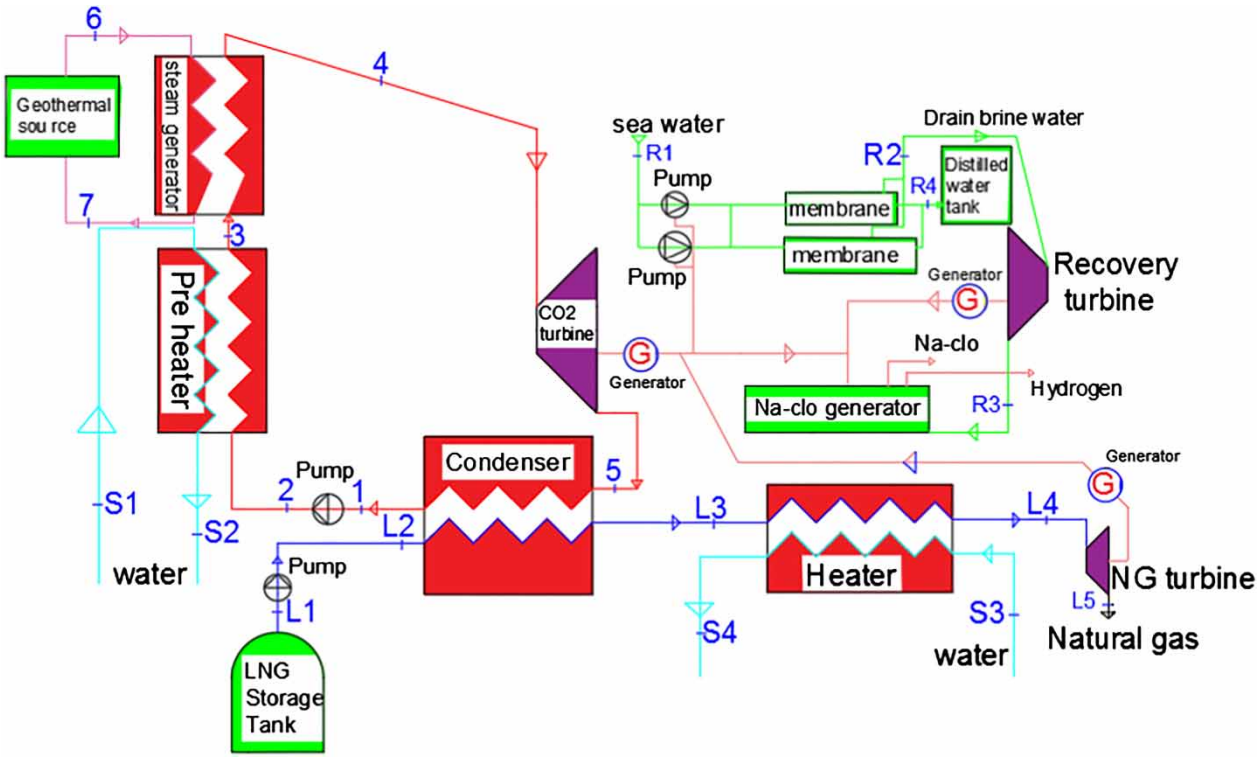

Figure 1 | A view of the model presented and investigated in this study.

carbon dioxide. The LNG operating fluid, passing through this complex, completes the gasification process and the output of the complex is natural gas. Its turbine is also used to generate power. So ultimately, by using this set of processes the heat is released from the carbon dioxide cycle, and power is generated in its turbine. Also, the gasification of the LNG is performed. Figure 2 presents the diagram of temperature in terms of the entropy of the power generation section of the model presented in this study.

In this model, all the net power generated by the turbines is converted into electrical power by the generators. The power generated is distributed with a specific ratio between reverse osmosis desalination and the sodium hypochlorite generator. Depending on the power produced in the model and the amount allocated to the desalination system, the inlet discharge of the desalination system and, consequently, the number of pressure chambers, will be determined. As mentioned before, the inputs of the sodium hypochlorite generator are a concentrated brine solution and electrical power. On the other hand, the discharge output is the concentrated

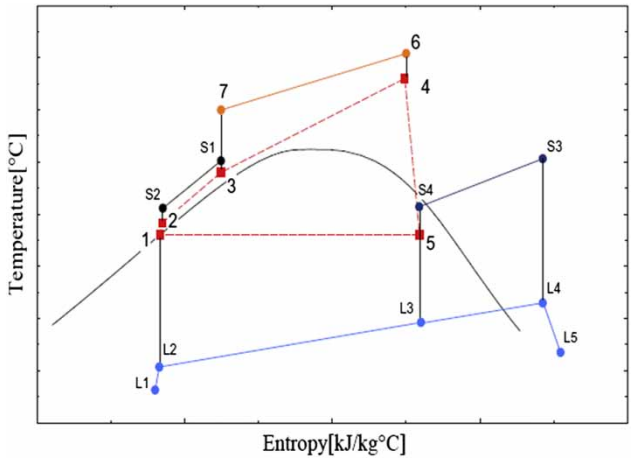

Figure 2 | Diagram of temperature in terms of the entropy of the power generation.

brine solution; this flow is considered as the input of the sodium hypochlorite system. So the power required by this generator is supplied from the power output of the model. Also, the discharge flow of the desalination system has a high pressure that is equivalent to the pressure of the pumps minus the pressure drop in the complex. Therefore,

Downloaded from http://iwaponline.com/ws/article-pdf/20/3/984/765699/ws020030984.pdf
by guest

this flow passes through the recovery turbine before it reaches the sodium hypochlorite generator and generates power. The generator also converts this power to electrical power and distributes it along with the carbon dioxide power and LNG for use in the model.

As mentioned, the inlet flow rate of the desalination system in this model is determined according to its input power. The input power of the sodium hypochlorite generator is also determined in terms of the discharge and its inlet flow concentration. The recovery turbine power generation is also dependent on the flow passing through it. The inlet flow discharge of the sodium hypochlorite generator and the discharge flow through the recovery turbine are also dependent on the discharge feeding flow of the desalination system. Thus, the percentage of desalination power consumption relative to generated power is dependent on the discharge of the sodium hypochlorite generator, or the desalination output. Therefore, the total product generated in this model is entirely dependent on the total net power generated by the CO_2 and natural gas turbines.

MATHEMATICAL THERMODYNAMICS OF MODEL

In order to undertake investigations of this study, the model must first be simulated by the governing thermodynamic equations. Each model section has its equations to obtain the values of the properties and energy transfer in different system flows and components. These equations are presented as follows.

Carbon dioxide power cycle

For all the components in this cycle, energy and mass balance have been taken into account. Other governing relationships are presented below.

Equation (1) calculates the heat transferred from the steam generator to carbon dioxide.

$$Q_{VG} = \dot{m}_{CO_2}(h_4 - h_3) \tag{1}$$

The carbon dioxide is heated by water in a preheater before entering the steam generator. The heat transferred to carbon dioxide in this preheater is calculated from Equation (2).

$$Q_{PH} = \dot{m}_{CO_2}(h_3 - h_2) \tag{2}$$

Carbon dioxide is also absorbed in the heat condenser. The amount of this heat is also obtained from Equation (3).

$$Q_{Condenser} = \dot{m}_{CO_2}(h_5 - h_1) \tag{3}$$

The mechanical power output of the turbine as well as the pump power required in the carbon dioxide cycle are calculated from Equations (4) and (5), respectively.

$$W_{Turb,CO_2} = \dot{m}_{CO_2}(h_4 - h_5) \tag{4}$$

$$W_{Pump,CO_2} = \dot{m}_{CO_2}(h_1 - h_2) \tag{5}$$

The turbine efficiency and pump efficiency in the carbon dioxide cycle are also calculated from Equations (6) and (7), respectively.

$$\eta_{Turb,CO_2} = \frac{h_4 - h_5}{h_4 - h_{5s}} \tag{6}$$

$$\eta_{Pump,CO_2} = \frac{h_{2s} - h_1}{h_2 - h_1} \tag{7}$$

Finally, the net power output of this cycle is calculated from Equation (8).

$$W_{Net,CO_2} = W_{Turb,CO_2} + W_{Pump,\,CO_2} \tag{8}$$

Flow of LNG

Energy and mass balance have been considered for all components in this flow. Other governing relationships are presented as follows.

The saturated LNG is first driven by the pump toward the condenser. It then enters the carbon dioxide cycle condenser and absorbs carbon dioxide heat. The value of this heat is equal to the amount of heat lost by the carbon dioxide in the condenser and can be calculated from Equation (3). This flow then enters the heater and receives heat from the water. The amount of heat received by this fluid

Downloaded from http://iwaponline.com/ws/article-pdf/20/3/984/765699/ws020030984.pdf
by guest

from the heater is calculated from Equation (9).

$$Q_{HT} = \dot{m}_{LNG}(h_{L4} - h_{L3}) \tag{9}$$

Eventually this flow passes through the natural gas turbine. The mechanical power output of the turbine and also the pump power required for LNG flow are calculated from Equations (10) and (11), respectively.

$$W_{Turb,NG} = \dot{m}_{LNG}(h_{L4} - h_{L5}) \tag{10}$$

$$W_{Pump,LNG} = \dot{m}_{LNG}(h_{L1} - h_{L2}) \tag{11}$$

The turbine efficiency and pump efficiency in this process are also calculated from Equations (12) and (13), respectively.

$$\eta_{Turb,NG} = \frac{h_{L4} - h_{L5}}{h_{L4} - h_{L5s}} \tag{12}$$

$$\eta_{Pump,LNG} = \frac{h_{L2s} - h_{L1}}{h_{L2} - h_{L1}} \tag{13}$$

The net power output of this cycle is calculated from Equation (14).

$$W_{Net,LNG} = W_{Turb,NG} + W_{Pump,\,LNG} \tag{14}$$

Reverse osmosis desalination and recovery turbines

Each desalination system is a set of pressure chambers fed by high-pressure pumps. Each pressure chamber also contains several elements or membranes that do not allow large particles, ions, and molecules with specific dimensions to pass. In this model, the number of elements and the amount of water produced vary with pressure in the system. Due to the high concentration of salt in the seawater used in this model for the desalination feed, a compressor chamber stage is typically used. One of the most critical parameters in desalination systems is the recovery ratio, which represents the percentage of feed water that is converted into drinking water. In this desalination model, a recovery ratio of 0.3 is used, and the water temperature is assumed to be constant for all stages. The governing equations in this section are presented below (Naseri *et al.* 2017a).

Equations (15) and (16) are obtained using mass balance and concentration balance.

$$\dot{m}_{FW} = \dot{m}_{PW} + \dot{m}_{BW} \tag{15}$$

$$\dot{m}_{FW}x_{FW} = \dot{m}_{PW}x_{PW} + \dot{m}_{BW}x_{BW} \tag{16}$$

In the above equations, $\dot{m}_{FW}$, $\dot{m}_{PW}$ and $\dot{m}_{BW}$ represent the feed water discharge, the outlet drinking water discharge and the discharge brine water discharge rate, respectively. Also x_{FW}, x_{PW}, and x_{BW} represent the concentration of feed brine water, the concentration of output drinking water and the concentration of discharge brine water, respectively.

According to the explanations given, the water supply discharge rate is obtained from Equation (17).

$$\dot{m}_{FW} = \frac{\dot{m}_{PW}}{RR} \tag{17}$$

As mentioned in the previous sections, osmotic pressure is defined for the phenomenon of osmosis. This pressure is equal to the pressure that must be applied to the flow to prevent osmotic flow. The osmotic pressure value for the three main flows is obtained from Equations (18)–(20) and the total osmotic pressure of the system is calculated based on Equation (21).

$$\pi_{FW} = RTx_{FW} \tag{18}$$

$$\pi_{PW} = RTx_{PW} \tag{19}$$

$$\pi_{BW} = RTx_{BW} \tag{20}$$

$$\Delta\pi = \left(\frac{\pi_{FW} + \pi_{BW}}{2}\right) - \pi_{PW} \tag{21}$$

In the above equations, R and T represent the global constants of gases and flow temperatures, respectively.

Knowing the concentration and temperature of discharge brine water, the water permeability coefficient is calculated by using Equation (22).

$$K_w = \frac{6.84 \times 10^{-8} \times [18.68 - (0.177 \times x_{BW})]}{T_{FW}} \tag{22}$$

Downloaded from http://iwaponline.com/ws/article-pdf/20/3/984/765699/ws020030984.pdf
by guest

Thus, the hydraulic pressure of the output water is obtained from Equation (23).

$$\Delta P = \frac{\dot{m}_{PW}}{K_w A_m} + \Delta\pi \tag{23}$$

where, A_m represents the area of the membrane.

Finally, taking into account the osmotic pressures and the path pressure drop, the total power required for desalination pumps is calculated from Equation (24).

$$W_{Net,RO} = \frac{\Delta P_{Net}\dot{m}_{FW}}{\rho_{FW}\eta_{RO.Pump}} \tag{24}$$

where, ρ_{FW}, $\eta_{RO.Pump}$ and ΔP_{Net} represent the feed water density, mechanical efficiency of the desalination pumps and the net pressure difference during the pumping process, respectively.

As mentioned earlier, the discharge water of the desalination system has a high pressure and so a recovery turbine is passed. The output power of this recovery turbine is calculated from Equation (25).

$$W_{Turb,Rec} = \dot{m}_{BW}(h_{R2} - h_{R3}) \tag{25}$$

Sodium hypochlorite generator

As mentioned earlier, a sodium hypochlorite generator requires a concentrated water and salt solution and electrical power, and one of the outputs of desalination in this model is a concentrated water and salt solution and also electrical power is produced in the model. In addition to releasing discharge brine water from the desalination outlet into free water, this has the disadvantages mentioned in the preceding sections. Therefore, the use of a sodium hypochlorite generator can be the right choice. The output of this system is also hydrogen gas and sodium hypochlorite solution. Equation (26) is obtained from the mass balance.

$$\dot{m}_{BW} = \dot{m}_{NaClO} + \dot{m}_{H_2} \tag{26}$$

where, $\dot{m}_{NaClO}$ and $\dot{m}_{H_2}$ represent the discharge rate of outlet sodium hypochlorite and the discharge rate of outlet hydrogen gas, respectively.

The temperature and concentration of the output solution of this system are obtained by using Equations (27) and (28), respectively (Neca CCPP 2008). The ratio of sodium hypochlorite concentration can vary according to its generator model and the efficiency of that generator in different systems.

$$T_{NaClO} = T_{BW} + 14 \tag{27}$$

$$x_{NaClO} = \frac{1}{6}x'_{BW} \tag{28}$$

In Equation (27), the temperature is in degrees C° or K.

The power consumption of the system is also calculated from Equation (29) (Neca CCPP 2008). This value can vary in different generators.

$$W_{NaClO\ Generator} = \frac{5.9 \times 3600 \times \dot{m}_{NaClO} \times \frac{x_{NaClO}}{1000}}{1.05} \tag{29}$$

MODELING ANALYSIS

Exergy analysis

The maximum useful work obtained from a system that relates only to its reference environment to achieve thermodynamic equilibrium with that environment is called exergy. One of the applications of exergy is the determination of exergy destruction due to irreversibility. Exergy can be divided into four parts: physical, chemical, kinetic, and potential. In this study, kinetic and potential exergy is ignored. Physical exergy is defined as the maximum theoretical useful work obtained as a system opposed to a balanced reference environment. Chemical exergy is related to the deviation and change of the chemical composition of a system relative to the chemical composition of its reference environment. Chemical exergy is considered for chemical fuels (Ahmadi *et al.* 2011).

In this study, only the physical exergy is calculated for all flows except the output flows of sodium hypochlorite generators, which also have chemical exergy due to changes in their chemical composition. The physical exergy of each system flow is calculated using Equation (30)

Downloaded from http://iwaponline.com/ws/article-pdf/20/3/984/765699/ws020030984.pdf
by guest

(Ahmadi *et al.* 2016b).

$$Ex_k = \dot{m}_k[(h_k - h_0) - T_0(s_k - s_0)] \quad (30)$$

where, T_0 is the reference ambient temperature and should be in Kelvin. In this respect, the subscript k represents the flow No. k. h_0 and s_0 are the enthalpy and entropy of the material for each flow under reference environment condition, respectively.

Chemical exergy of the outlet flows of the sodium hypochlorite generator are calculated using their standard chemical exergy and is calculated from Equations (31) and (32) (Bejan *et al.* 1996; Ferreira 2013).

$$Ex_{ch,\,NaClO} = \frac{\dot{m}_{NaClO} \times \frac{x_{NaClO}}{1000} \times 170.17 \times 1000}{MW_{NaClO}} \quad (31)$$

$$Ex_{ch,\,H_2} = \frac{\dot{m}_{H_2} \times 236.1 \times 1000}{MW_{H_2}} \quad (32)$$

where, the standard chemical exergy of sodium hypochlorite is 170.17 kJ/mol and the standard chemical exergy of hydrogen is 236.1 kJ/mol. MW_{NaClO} and MW_{H_2} represent the molar mass of sodium hypochlorite and the molar mass of hydrogen, respectively. To calculate the exergy of these two flows, the sum of their chemical and physical exergies must be calculated.

To evaluate the system components, we calculate their exergy destruction. Equations (33)–(38) calculate exergy destruction in the various components of the model under investigation. Equation (33) is associated with a variety of heat exchangers and condensers.

$$I_{Hx,Condenser} = \sum Ex_{in} - \sum Ex_{out} \quad (33)$$

$$I_{Turb} = Ex_{in} - Ex_{out} - W_{Turb} \quad (34)$$

$$I_{Pump} = Ex_{in} - Ex_{out} + W_{Pump} \quad (35)$$

$$I_{generator} = W_{in,mech} - W_{out,elec} \quad (36)$$

$$I_{Ro\ system} = Ex_{in} - \sum Ex_{out} + W_{in,elec} \quad (37)$$

$$I_{NaClO\ generator} = Ex_{in} - \sum Ex_{out} + W_{in,elec} \quad (38)$$

The exergy destruction relationships for each of the model components of this study are presented in Table 1.

Equation (39) is obtained according to the exergy balance that is obtained for each component of the process:

$$Ex_{F,k} = Ex_{P,k} + Ex_{D,k} \quad (39)$$

where, $Ex_{F,k}$ and $Ex_{P,k}$ are respectively the exergy fuel of the k-th component and the exergy product of the k-th component, respectively. Table 2 presents the exergy product relationships for each of the model components of this study.

The exergy efficiency of each component is also defined as in Equation (40):

$$\varepsilon_k = \frac{Ex_{P,k}}{Ex_{F,k}} = 1 - \frac{Ex_{D,k}}{Ex_{F,k}} \quad (40)$$

Advanced exergy analysis

By evaluating advanced exergy, we can determine the certain minimum level of exergy destruction. In the case of advanced exergy analysis, the exergy destruction of components is broken into two parts: avoidable and unavoidable. In another case, it is broken into two parts: endogenous exergy

Table 1 | Relationships of exergy destruction for all model components

$I_{VG} = Ex_3 + Ex_6 - Ex_4 - Ex_7$
$I_{Preheater} = Ex_2 + Ex_{s1} - Ex_3 - Ex_{s2}$
$I_{Turb,CO_2} = Ex_4 - Ex_5 - W_{Turb,CO_2}$
$I_{Gen\ Turb,CO_2} = W_{Turb,CO_2} - W_{elec\ Turb,CO_2}$
$I_{Condenser} = Ex_5 + Ex_{L2} - Ex_1 - Ex_{L3}$
$I_{Pump,CO_2} = Ex_1 - Ex_2 + W_{Pump,CO_2}$
$I_{Pump,LNG} = Ex_{L1} - Ex_{L2} - W_{Pump,LNG}$
$I_{HT} = Ex_{L3} + Ex_{s3} - Ex_{L4} - Ex_{s4}$
$I_{Turb,NG} = Ex_{L4} - Ex_{L5} - W_{Turb,NG}$
$I_{Gen\ Turb,NG} = W_{Turb,NG} - W_{elec\ Turb,NG}$
$I_{RO} = Ex_{R1} - Ex_{R2} - Ex_{R4} + W_{net,RO}$
$I_{Rec\ Turb} = Ex_{R2} - Ex_{R3} - W_{Rec\ Turb}$
$I_{Gen\ Rec\ Turb} = W_{Rec\ Turb} - W_{elec\ Rec\ \ Turb}$
$I_{NaClO\ generator} = Ex_{R3} - Ex_{H2} - Ex_{NaClO} + W_{NaClO\ generator}$

Downloaded from http://iwaponline.com/ws/article-pdf/20/3/984/765699/ws020030984.pdf
by guest

Table 2 | Exergy product relationships for all model components

$Ex_{P,VG} = Ex_4 - Ex_3$
$Ex_{P,Preheater} = Ex_{s2} - Ex_{s1}$
$Ex_{P,Turb,CO_2} = W_{Turb,CO_2}$
$Ex_{P,Gen\ Turb,CO_2} = W_{elec\ Turb,CO_2} = \eta_{Gen} \times W_{Turb,CO_2}$
$Ex_{P,Condenser} = Ex_1 - Ex_5$
$Ex_{P,Pump,CO_2} = Ex_2 - Ex_1$
$Ex_{P,HT} = Ex_{s4} - Ex_{s3}$
$Ex_{P,Turb,NG} = W_{Turb,NG}$
$Ex_{P,Pump,LNG} = Ex_{L2} - Ex_{L1}$
$Ex_{P,Gen\ Turb,NG} = W_{elec\ Turb,NG}$
$Ex_{P,RO} = Ex_{R2} + Ex_{R4} - Ex_{R1}$
$Ex_{P,Rec\ Turb} = W_{Rec\ Turb}$
$Ex_{P,Gen\ Rec\ Turb} = W_{elec\ Rec\ \ Turb}$
$Ex_{P,NaClO\ generator} = Ex_{H2} + Ex_{NaClO}$

destruction and exogenous exergy destruction. This is done to evaluate better its components and how to improve the performance of the system.

Endogenous exergy destruction is a part of exergy destruction that is related to the component, and it is not the result of its interactions with other components to calculate the endogenous exergy of each component. It is assumed that the other components work ideally, and only the considered component is under its real condition. When the exergy of the desired component is calculated in this case, the value obtained is the endogenous exergy of the considered component. Then, considering Equation (41), according to the difference of the exergy destruction and the endogenous exergy destruction of each component, the exogenous exergy destruction of that component is calculated (Petrakopoulou *et al.* 2012).

$$Ex_{D,k} = Ex_{D,k}^{EN} + Ex_{D,k}^{EX} \tag{41}$$

where, $Ex_{D,k}^{EN}$ and $Ex_{D,k}^{EX}$ represent the endogenous exergy destruction of component k and the exogenous exergy destruction of component k, respectively.

Unavoidable exergy destruction cannot be reduced due to technical limitations, such as material properties, production costs and production methods. But avoidable exergy destruction can be reduced by improvement in the design of the component (Galindo *et al.* 2016).

In order to calculate the unavoidable exergy destruction of a component, consider the desired component apart from the rest, with the most favorable operating conditions. These conditions are associated with minimum exergy destruction and are related to low-temperature differences and low thermal and compressive losses in the components. The assumptions to simulate certain conditions depend on the decision-maker and are somewhat tentative. These assumptions can be selected on the basis of knowledge and experience about the factory and technical operations. Considering the maximum improvement potential, it can be achieved for any part of the process in the predictable future (Petrakopoulou *et al.* 2012). When the exergy destruction and the exergy product of that component are calculated by considering these conditions for the component, the unavoidable exergy destruction of the component can be calculated by using Equation (42). Then, according to Equation (43) of the difference between the exergy destruction and the unavoidable exergy destruction of each component, the unavoidable exergy destruction of that component is calculated (Galindo *et al.* 2016).

$$Ex_{D,k}^{UN} = Ex_{P,k} \times \left(\frac{Ex_D}{Ex_P}\right)_k^{UN} \tag{42}$$

$$Ex_{D,k} = Ex_{D,k}^{UN} + Ex_{D,k}^{AV} \tag{43}$$

Table 3 presents the unavoidability and ideal conditions for the different model components of this study (Fallah *et al.* 2016).

For the ideal case in the sodium hypochlorite generator, it is assumed that all salts present in the inlet flow contribute to the chemical reaction and generate the product. Therefore, the sodium hypochlorite concentration in the output solution of this system in the ideal state would be 24.4 kg/m^3. On the

Table 3 | Unavoidability and ideal conditions

Equipment	Ideal	Unavoidability
Heat exchanger	$\Delta P = 0$ $\Delta T_{min} = 0$	$\Delta P = 1\%$ $\Delta T_{min} = 3$
Turbine	$\eta_s = 1$	$\eta_s = 0.95$
Pump	$\eta_s = 1$	$\eta_s = 0.95$
Condenser	$\Delta P = 0$ $\Delta T_{min} = 0$	$\Delta P = 0.5\%$ $\Delta T_{min} = 3$
Generator	$\eta_g = 1$	$\eta_g = 0.99$

Downloaded from http://iwaponline.com/ws/article-pdf/20/3/984/765699/ws020030984.pdf
by guest

other hand, by obtaining the system reaction enthalpy, the energy required for the output of each kg of pure hypochlorite sodium in the ideal mode is calculated to be 1.6642 kW. For unavoidable conditions, for this generator, the maximum concentration for the output solution of this system is 25% of the water and salt concentration of the system, which is about 16% of the water and salt concentration of the system in the normal state. Also, the power consumption of this system per kg of sodium hypochlorite in the unavoidable conditions is considered to be 70% of the real conditions.

For the desalination system as well, the system pumps comply with Table 3 for both ideal and unavoidable conditions. Another parameter in this system is desalination, which indicates that the concentration of outlet drinking water has decreased by a few percent compared to the discharge water concentration. In the normal state, this is 99%. The desalination in the ideal state can be 100%.

RESULTS

After modeling and the first step of exergy analysis, the thermodynamic and exergy properties of all flows are determined. This information has been provided in Table 4.

Then, the values of fuel exergy, product exergy, exergy destruction and finally exergy efficiency are calculated for all process components by exergy analysis. These values are presented in Table 5.

The highest exergy efficiency is associated with generators. This is more than 95% for generators. After generators, the highest exergy efficiency was observed for natural gas turbines at 0.7726. The lowest value of exergy efficiency is related to the heater and its value is 0.1391.

With advanced exergy analysis, the exergy destruction of the components is broken into two parts: unavoidable and avoidable. And in another way, it breaks down into two

Table 4 | Thermodynamic properties of all flows

Number of flow	Working fluid	Temperature (C°)	Pressure (Mpa)	Enthalpy (kj/kg)	Flow rate (kg/s)	Exergy (kW)
1	CO_2	−53.12	0.60	86.79	6.73	1,565.50
2	CO_2	−48.24	12.49	99.55	6.73	1,628.10
3	CO_2	−10.00	12.24	174.03	6.73	1,514.20
4	CO_2	120.00	12.00	519.68	6.73	1,684.60
5	CO_2	−52.63	0.61	431.63	6.73	747.60
L1	LNG	−161.47	0.1014	0.04	4.5	4,860.40
L2	LNG	−157.89	6.58	21.86	4.5	4,881.80
L3	LNG	−62.63	6.44	538.08	4.5	3,111.10
L4	LNG	10.00	6.31	806.36	4.5	2,806.10
L5	NG	−17.86	4.00	762.27	4.5	2,549.30
S3	Water	25.00	0.10	104.92	14.41	0.00
S4	Water	5.00	0.099	21.11	14.41	42.41
S1	Water	25.00	0.10	104.92	5.98	0.00
S2	Water	5.00	0.09	21.11	5.98	17.62
6	Water	140.00	0.70	589.38	10.00	754.98
7	Water	85.00	0.68	365.51	10.00	229.15
R1	Sea water	25.00	0.10	99.89	5.80	0.00
R2	Brine	25.00	6.89	106.45	4.10	29.44
R3	Brine	25.00	0.30	101.35	4.10	6.08
R4	Distilled water	25.00	0.10	104.92	1.69	0.00
H2	H2	25.00	0.10	0.00	7e-4	82.95
NaClO	NaCLo	39.00	0.25	163.57	4.10	68.16

Downloaded from http://iwaponline.com/ws/article-pdf/20/3/984/765699/ws020030984.pdf
by guest

Table 5 | Fuel exergy, product exergy, exergy destruction and finally exergy efficiency

Equipment	$Ex_{F,k}$	$Ex_{P,k}$	$Ex_{D,k}$	$\varepsilon_k = \frac{Ex_{P,k}}{Ex_{F,k}}$
Steam generator	528.82	170.37	355.45	0.3222
CO_2 turbine	936.9	593.18	343.72	0.6331
Condenser	1,770.69	817.81	952.88	0.4519
CO_2 pump	85.9	62.56	23.34	0.7283
Preheater	113.84	17.62	96.22	0.1548
LNG pump	98.17	21.34	76.83	0.2174
Heater	304.92	42.41	262.51	0.1391
NG turbine	256.86	198.44	58.42	0.7726
CO_2 turbine generator	506.46	481.91	25.36	0.9515
NG turbine generator	100.25	95.24	5.01	0.9500
NaClO generator	555.29	151.12	404.17	0.2721
Desalination	47.69	29.44	18.28	0.6173
Recovery turbine	21.94	20.90	2.45	0.9523
Recovery turbine generator	20.89	19.85	1.04	0.9502

parts: endogenous exergy destruction and exogenous exergy destruction. These values are presented in Table 6.

According to the results presented in Table 6, it is observed that in components such as the steam generator, condenser, heater, preheater, desalination and recovery turbine, the unavoidable exergy destruction is higher than the avoidable part. Therefore, we cannot achieve significant improvements in reducing the exergy destruction of these components. When exergy analysis is performed routinely, it is found that the exergy destruction in the condenser is much greater than in the other components; in the meantime, if advanced exergy analysis is not performed, it may be selected to improve the total exergy destruction of the condenser system. But with advanced exergy analysis, it is found that most of the exergy destruction in this component is unavoidable and almost impossible to improve. The sodium hypochlorite generator also has higher exergy destruction than other components, about 60% of which is unavoidable. However, 40% of its exergy destruction is removable; given its large amount, the exergy destruction in this component is not low and it can be worth selecting for improvement. In both desalination and recovery turbines, the exergy destruction is low compared to other components and at the same time has a greater unavoidable share. Therefore, they cannot be used to improve the process. One of the best options for improving exergy destruction is the carbon dioxide turbine because it has more exergy destruction than other components and yet most of it, about 88%, is avoidable and can be improved. In pumps and turbines related to LNG flow, the avoidable part accounts for 3% and 20% of the exergy destruction of these components, respectively. Generators also have a greater share of the avoidable part.

Table 6 | Advanced exergy result

Equipment	$Ex_{D,k}$	$Ex_{D,k}^{UN}$	$Ex_{D,k}^{AV}$	$Ex_{D,k}^{EN}$	$Ex_{D,k}^{EX}$
Steam generator	355.45	278.31	57.14	264.39	91.15
CO_2 turbine	343.72	42.21	301.51	436.87	−93.15
Condenser	952.88	879.78	73.1	1,062.2	−109.3
CO_2 pump	23.34	4.96	18.38	26.12	−2.78
Preheater	96.22	56.91	39.31	93.86	2.36
LNG pump	76.83	3.22	73.61	71.88	4.95
Heater	262.51	227.52	34.99	167.57	94.94
NG turbine	58.42	12.37	46.05	57.72	0.7
CO_2 turbine generator	25.36	4.86	20.5	51	−25.64
NG turbine generator	5.01	0.96	4.05	9.76	−4.75
NaClO generator	404.17	242.6	161.57	840	−435.83
Desalination	18.28	10.67	7.61	37.92	−19.64
Recovery turbine	2.45	2.07	0.38	5.15	−2.7
Recover turbine generator	1.04	0.20	0.84	2.77	−1.73

According to Table 6, it can be seen that the exogenous part of exergy destruction for some of the components is negative. This means that the endogenous part of the exergy destruction is greater than the actual exergy destruction of these components, the reason being that when ideal conditions are used for the other components for computing the endogenous part of the exergy destruction, the discharge rate in some components changes and increases and as a result, the calculated destruction exergy will be greater than the actual destruction exergy.

CONCLUSION

In this study, modeling, exergy, and advanced exergy analyses were performed for a model of seawater desalination and co-generation of sodium hypochlorite. The power required in this model was provided by the organic carbon dioxide

Downloaded from http://iwaponline.com/ws/article-pdf/20/3/984/765699/ws020030984.pdf
by guest

power cycle and the liquefied natural gas gasification cycle for the conversion of liquefied natural gas and heat capture from carbon dioxide. Geothermal energy was also used as the heat source of the carbon dioxide cycle. The pressure used in the desalination process for desalination of salt water was also used to generate more power in a recovery turbine. The summary of the important results obtained in this study is as follows:

By performing the usual exergy analysis and advanced exergy analysis it is concluded that to study the system conditions and reduce its exergy destruction, routine analysis and consideration of exergy destruction of each component alone is not sufficient and with advanced exergy analysis it is possible to the percentage and amount of exergy destruction of each component that can be improved. In this model, the best option to improve exergy destruction is the carbon dioxide turbine. This means that increasing the efficiency of this turbine will greatly improve the exergy destruction of the system. The next suitable options for this are the turbine and liquid natural gas cycle pump and sodium hypochlorite generator.

REFERENCES

Abbassi, M. A., Safaei, M. R., Djebali, R., Guedri, K., Zeghmati, B. & Alrashed, A. A. 2018 LBM simulation of free convection in a nanofluid filled incinerator containing a hot block. *International Journal of Mechanical Sciences* **144**, 172–185.

Abdollahi, A., Darvanjooghi, M. H. K., Karimipour, A. & Safaei, M. R. 2018 Experimental study to obtain the viscosity of CuO-loaded nanofluid: effects of nanoparticles' mass fraction, temperature and basefluid's types to develop a correlation. *Meccanica* **53** (15), 3739–3757.

Ahmadi, P., Dincer, I. & Rosen, M. A. 2011 Exergy, exergoeconomic and environmental analyses and evolutionary algorithm based multi-objective optimization of combined cycle power plants. *Energy* **36** (10), 5886–5898.

Ahmadi, M. H., Mehrpooya, M. & Pourfayaz, F. 2016a Thermodynamic and exergy analysis and optimization of a transcritical CO_2 power cycle driven by geothermal energy with liquefied natural gas as its heat sink. *Applied Thermal Engineering* **109**, 640–652.

Ahmadi, M. H., Mehrpooya, M. & Pourfayaz, F. 2016b Exergoeconomic analysis and multi objective optimization of performance of a carbon dioxide power cycle driven by geothermal energy with liquefied natural gas as its heat sink. *Energy Conversion and Management* **119**, 422–434.

Ahmadi, M. H., Mohammadi, A., Pourfayaz, F., Mehrpooya, M., Bidi, M., Valero, A. & Uson, S. 2016c Thermodynamic analysis and optimization of a waste heat recovery system for proton exchange membrane fuel cell using transcritical carbon dioxide cycle and cold energy of liquefied natural gas. *Journal of Natural Gas Science and Engineering* **34**, 428–438.

Akrami, E., Chitsaz, A., Nami, H. & Mahmoudi, S. M. S. 2017 Energetic and exergoeconomic assessment of a multi-generation energy system based on indirect use of geothermal energy. *Energy* **124**, 625–639.

Al-Mutaz, I. S. 1991 Environmental impact of seawater desalination plants. *Environmental Monitoring and Assessment* **16** (1), 75–84.

Arani, A. A. A., Akbari, O. A., Safaei, M. R., Marzban, A., Alrashed, A. A., Ahmadi, G. R. & Nguyen, T. K. 2017 Heat transfer improvement of water/single-wall carbon nanotubes (SWCNT) nanofluid in a novel design of a truncated double-layered microchannel heat sink. *International Journal of Heat and Mass Transfer* **113**, 780–795.

Behnampour, A., Akbari, O. A., Safaei, M. R., Ghavami, M., Marzban, A., Shabani, G. A. S. & Mashayekhi, R. 2017 Analysis of heat transfer and nanofluid fluid flow in microchannels with trapezoidal, rectangular and triangular shaped ribs. *Physica E: Low-Dimensional Systems and Nanostructures* **91**, 15–31.

Bejan, A., Tsatsaronis, G. & Moran, M. 1996 *Thermal Design and Optimization*. John Wiley & Sons, Inc., Hoboken, NJ, 542 pp.

Dadsetani, R., Sheikhzadeh, G. A., Safaei, M. R., Alnaqi, A. A. & Amiriyoon, A. 2019 Exergoeconomic optimization of liquefying cycle for noble gas argon. *Heat and Mass Transfer* **55** (7), 1995–2007.

Fallah, M., Mahmoudi, S. M. S., Yari, M. & Ghiasi, R. A. 2016 Advanced exergy analysis of the Kalina cycle applied for low temperature enhanced geothermal system. *Energy Conversion and Management* **108**, 190–201.

Ferreira, G. (ed.) 2013 *Alternative Energies: Updates on Progress*, Vol. 34. Springer Science & Business Media, Berlin, Germany.

Galindo, J., Ruiz, S., Dolz, V. & Royo-Pascual, L. 2016 Advanced exergy analysis for a bottoming organic Rankine cycle coupled to an internal combustion engine. *Energy Conversion and Management* **126**, 217–227.

Hoseinzadeh, S. 2019 Thermal performance of electrochromic smart window with nanocomposite structure under different climates in Iran. *Micro and Nanosystems* **11** (2), 154–164. https://doi.org/10.2174/1876402911666190218145433.

Hoseinzadeh, S. & Azadi, R. 2017 Simulation and optimization of a solar-assisted heating and cooling system for a house in Northern of Iran. *Journal of Renewable and Sustainable Energy* **9** (4), 045101. doi:10.1063/1.5000288.

Hoseinzadeh, S., Heyns, P. S., Chamkha, A. J. & Shirkhani, A. 2019a Thermal analysis of porous fins enclosure with the comparison of analytical and numerical methods. *Journal of Thermal Analysis and Calorimetry* **138**, 727–735. doi:10.1007/s10973-019-08203-x.

Hoseinzadeh, S., Moafi, A., Shirkhani, A. & Chamkha, A. J. 2019b Numerical validation heat transfer of rectangular

Downloaded from http://iwaponline.com/ws/article-pdf/20/3/984/765699/ws020030984.pdf
by guest

cross-section porous fins. *Journal of Thermophysics and Heat Transfer* **33** (3), 1–7.

Hoseinzadeh, S., Hadi Zakeri, M., Shirkhani, A. & Chamkha, A. J. 2019c Analysis of energy consumption improvements of a zero-energy building in a humid mountainous area. *Journal of Renewable and Sustainable Energy* **11** (1), 015103. doi:10.1063/1.5046512.

Hoseinzadeh, S., Heyns, P. S. & Kariman, H. 2019d Numerical investigation of heat transfer of laminar and turbulent pulsating Al_2O_3/water nanofluid flow. *International Journal of Numerical Methods for Heat & Fluid Flow* **30** (3), 1149–1166.

Javadi, M. A., Hoseinzadeh, S., Khalaji, M. & Ghasemiasl, R. 2019 Optimization and analysis of exergy, economic, and environmental of a combined cycle power plant. *Sadhana – Academy Proceedings in Engineering Sciences* **44** (5), 121. https://doi.org/10.1007/s12046-019-1102-4

Kariman, H., Hoseinzadeh, S. & Heyns, P. S. 2019a Energetic and exergetic analysis of evaporation desalination system integrated with mechanical vapor recompression circulation. *Case Studies in Thermal Engineering* **16**, 100548.

Kariman, H., Hoseinzadeh, S., Shirkhani, A., Heyns, P. S. & Wannenburg, J. 2019b Energy and economic analysis of evaporative vacuum easy desalination system with brine tank. *Journal of Thermal Analysis and Calorimetry* 1–10. https://doi.org/10.1007/s10973-019-08945-8.

Keshavarzzadeh, A. H., Ahmadi, P. & Safaei, M. R. 2019 Assessment and optimization of an integrated energy system with electrolysis and fuel cells for electricity, cooling and hydrogen production using various optimization techniques. *International Journal of Hydrogen Energy* **44** (39), 21379–21396.

Mahmoudi, S. M. S. & Ghavimi, A. R. 2016 Thermoeconomic analysis and multi objective optimization of a molten carbonate fuel cell–supercritical carbon dioxide–organic Rankin cycle integrated power system using liquefied natural gas as heat sink. *Applied Thermal Engineering* **107**, 1219–1232.

Maleki, H., Safaei, M. R., Alrashed, A. A. & Kasaeian, A. 2019 Flow and heat transfer in non-Newtonian nanofluids over porous surfaces. *Journal of Thermal Analysis and Calorimetry* **135** (3), 1655–1666.

Mehrpooya, M., Sharifzadeh, M. M. M. & Rosen, M. A. 2016 Energy and exergy analyses of a novel power cycle using the cold of LNG (liquefied natural gas) and low-temperature solar energy. *Energy* **95**, 324–345.

Naseri, A., Bidi, M. & Ahmadi, M. H. 2017a Thermodynamic and exergy analysis of a hydrogen and permeate water production process by a solar-driven transcritical CO_2 power cycle with liquefied natural gas heat sink. *Renewable Energy* **113**, 1215–1228.

Naseri, A., Bidi, M., Ahmadi, M. H. & Saidur, R. 2017b Exergy analysis of a hydrogen and water production process by a solar-driven transcritical CO_2 power cycle with Stirling engine. *Journal of Cleaner Production* **158**, 165–181.

Neca CCPP 2008 Contract No. (HIR-NK-CT/WE-014).

Petrakopoulou, F., Tsatsaronis, G., Morosuk, T. & Carassai, A. 2012 Conventional and advanced exergetic analyses applied to a combined cycle power plant. *Energy* **41** (1), 146–152.

Safaei, M. R., Jahanbin, A., Kianifar, A., Gharehkhani, S., Kherbeet, A. S., Goodarzi, M. & Dahari, M. 2016 Mathematical modeling for nanofluids simulation: a review of the latest works. *Modeling and Simulation in Engineering Sciences*. doi: 10.5772/64154.

Sarafraz, M. M., Tlili, I., Tian, Z., Bakouri, M. & Safaei, M. R. 2019a Smart optimization of a thermosyphon heat pipe for an evacuated tube solar collector using response surface methodology (RSM). *Physica A: Statistical Mechanics and its Applications* **534**, 122146.

Sarafraz, M. M., Tlili, I., Abdul Baseer, M. & Safaei, M. R. 2019b Potential of solar collectors for clean thermal energy production in smart cities using nanofluids: experimental assessment and efficiency improvement. *Applied Sciences* **9** (9), 1877.

Sun, Z., Wang, J., Dai, Y. & Wang, J. 2012 Exergy analysis and optimization of a hydrogen production process by a solar-liquefied natural gas hybrid driven transcritical CO_2 power cycle. *International Journal of Hydrogen Energy* **37** (24), 18731–18739.

Wang, J., Sun, Z., Dai, Y. & Ma, S. 2010 Parametric optimization design for supercritical CO_2 power cycle using genetic algorithm and artificial neural network. *Applied Energy* **87** (4), 1317–1324.

Wang, J., Wang, J., Dai, Y. & Zhao, P. 2014 Thermodynamic analysis and optimization of a transcritical CO_2 geothermal power generation system based on the cold energy utilization of LNG. *Applied Thermal Engineering* **70** (1), 531–540.

Xia, G., Sun, Q., Cao, X., Wang, J., Yu, Y. & Wang, L. 2014 Thermodynamic analysis and optimization of a solar-powered transcritical CO_2 (carbon dioxide) power cycle for reverse osmosis desalination based on the recovery of cryogenic energy of LNG (liquefied natural gas). *Energy* **66**, 643–653.

Yousef Nezhad, M. E. & Hoseinzadeh, S. 2017 Mathematical modelling and simulation of a solar water heater for an aviculture unit using MATLAB/SIMULINK. *Journal of Renewable and Sustainable Energy* **9** (6), 063702. https://doi.org/10.1063/1.5010828.

First received 11 July 2019; accepted in revised form 24 January 2020. Available online 10 February 2020

Downloaded from http://iwaponline.com/ws/article-pdf/20/3/984/765699/ws020030984.pdf
by guest